Chapter 6 Appendix I. Compact high spectral resolution polychromator for $ClONO_2$ measurements

- A 0.1 cm^{-1} spectral resolution polychromator by combination of an echelle grating and aspherical mirrors -

$ClONO_2$ is one of the most important species governing the chemistry of stratosphere, especially O_3 depletion, particularly in the polar regions. A compact echelle grating spectrometer (f=200 mm) with 0.2 cm^{-1} spectral resolution around the 780.2 cm^{-1} chlorine nitrate ($ClONO_2$) absorption band has been designed and tested. This is a part of the flight model of the Improved Limb Atmospheric Spectrometer-II (ILAS-II) mission onboard Advanced Earth Observing Satellite-II (ADEOS-II). Using an off axis parabolic collimator and two cylindrical off axis parabolic collecting mirrors, this spectrometer is a compact space-borne instrument optimized for solar occultation measurements. The solar absorption spectra measured with the array detector on the ground are consistent with the designed spectral resolution and the resolution simulated with the Code V optical performance simulator. Radiometric and spectrometric pre-launch calibration results of the spectrometer are discussed. The instrument slit function measurement with a tunable diode laser and integrating sphere is also discussed.[1]

[1] This chapter has been published in "Design and performance of ILAS-II echelle grating spectrometer for $ClONO_2$ measurement," **SPIE 3437**, 240-248 (1998) and was co-authored by M. Suzuki, K. Nakamura and Y. Sasano. It was revised and updated.

6.1. Introduction and Objectives of the Development

For the remote sensing of atmosphere in the infrared (IR) region, high spectral resolution (< 0.1 cm^{-1}) is usually required. $ClONO_2$ is one of the most important species governing the chemistry of stratosphere, especially O_3 depletion, particularly in the polar regions [*Solomon et al.*, 1986 and *Webster et al.*, 1993]. $ClONO_2$ has been observed by the space shuttle-borne spectrometer ATMOS and the balloon-borne spectrometers such as LPMA and MIPAS-B [*Rhineland et al.*, 1994, *Massie et al.*, 1987, *Camy-Peyret et al.*, 1995, and *T. v. Clarmann et al.*, 1997]. These instruments are Michelson Fourier transform spectrometers (FTS), which have a spectral resolution higher than 0.1 cm^{-1} in order to detect the spectra of several trace gases including the narrow spectra of gases other than $ClONO_2$. Although FTS is a common instrument in laboratories and balloon-borne measurements, it is not practical to use FTS for solar occultation observation on unmanned spacecraft, due to the severe environmental conditions. Because the spectral resolution of FTS is proportional to optical path difference (mirror moving displacements), high spectral resolution is achieved at the expense of large instrument size and long measurement time. For absorption spectrum measurements of specific atmospheric molecules such as $ClONO_2$ from satellites, measurements with echelle grating spectrometers, which are discussed here, are the only feasible ways of taking account the limited resources and constraints (power consumption, weight, and size) and rapid measuring intervals.

This chapter reports on the design and instrumentation of a compact echelle grating spectrometer. The spectrometer is optimized for Instantaneous Field of View (IFOV) limited measurement to achieve high spectral resolution in a limited spectral region. It consists of one of the coarsest IR echelle gratings available (23.2 grooves/mm), and a combination of two off-axis cylindrical mirrors. The solar absorption spectra of H_2O and CO_2 with this compact echelle grating spectrometer and a Mercury Cadmium Telluride (MCT) detector on the ground were measured. The result shows high spectral resolution (0.19 m^{-1}) with high SNR (approximately 1000). The echelle spectrometer discussed here is a part of the Improved Limb Atmospheric Spectrometer-II (ILAS-II) [*M. Suzuki et al.*, 1995]. The ILAS-II is a solar occultation grating spectrometer, developed by the Environment Agency of Japan, and due to be placed in an 803 km sun-synchronous polar orbit in 2002, with a local equator crossing time of 10:30 am. The ILAS-II is the successor of the ILAS, which was onboard Advanced Earth Observing Satellite (ADEOS) from August 1996 [*M. Suzuki et al.*, 1994].

6.2. Design and Instrumentation

(1) Requirements

$ClONO_2$ has a baseline like absorption peak at 780.2 cm^{-1} (ν_4 band) Q branch. An example of transmission spectra of $ClONO_2$, CO_2 and O_3 using the solar occultation technique from satellites is shown in Figure 6-1. The sensitivity was determined using the atmospheric optical calculation code FASCODE and the HITRAN92 absorption cross sections of $ClONO_2$ assuming the US standard atmosphere and a mid-latitude $ClONO_2$ vertical profile measured by ATMOS, which is one of the lowest measured densities of $ClONO_2$ [*Clough et al.*, 1986 and *Rothman et al.*, 1992]. The result shows that a 0.2 cm^{-1} spectral resolution is

sufficient to detect the strong $ClONO_2$ absorption peak at 780.2 cm^{-1}. The requirements for the instrument are as follows.

(a) 0.2 cm^{-1} spectral resolution

(b) 1 km vertical height resolution (rapid sampling intervals)

(c) Solar disk light source

(d) Small size and light weight

(e) Low cost (use of uncooled detector)

The above points (b) and (c) are requirements for IFOV. The IFOV is specified to maximize the collected input flux while maintaining the 1 km vertical tangent height resolution. For these purposes, the horizontal field of view is 6.69 mrad, which is nearly equal to the radius of the solar disk and the vertical field of view is 0.308 mrad, which is equal to a 1 km tangent height in the observation geometry. The assumed foreoptics telescope aperture and focal length are 130 mm and 600 mm, respectively, limited by the practical sizes for space-borne instruments. Hence the image of the observation target is focused on a 4.015 by 0.185 mm entrance slit.

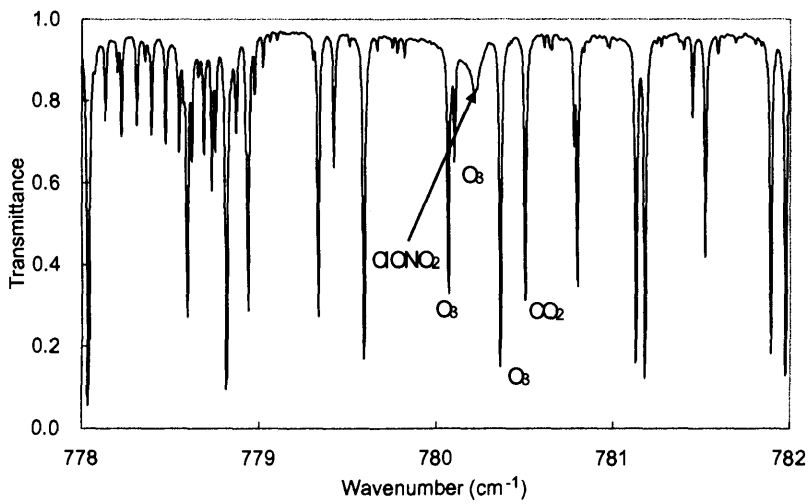

Figure 6-1. $ClONO_2$ 780.2 cm^{-1} (12.817μm) Q-branch absorption spectra in the north polar region in March. Note that the tangent height is 20 km. The one dimensional array detector covers the baseline-like absorption $ClONO_2$ over 779-781 cm^{-1}.

Table 6-1. Specification of the echelle grating spectrometer.

Target	$ClONO_2$
Wavelength region	12.783-12.851 μm (778.2−782.4 cm^{-1})
Center wavelength	12.8172 μm (780.20 cm^{-1})
Spectral resolution	0.2 cm^{-1}
IFOV	6.690×0.3083 mrad
Entrance slit	0.185±0.01 mm × 4.015 ± 0.05 mm
Echelle Grating Number of grooves Blaze angle	 23.20±0.10/mm 65.1±1 deg
Detector Size and Number of pixels	MCT detector: 0.08 (interval 0.1)×1.0 mm, 20 pixels Pyroelectric detector: 0.18 (interval 0.2)×1.0 mm, 22 pixels

Detectors, especially photon detectors with a mechanical cooler, are usually expensive components for IR space-borne instruments. Photon detectors with a cooler also consume power in orbit and add weight. Although thermal detectors, such as pyroelectric ones, can be operated under room temperature, they are less sensitive than photon detectors. In this spectrometer either an MCT detector attached to a liquid-nitrogen cooled dewar or a $PbTiO_3$ pyroelectric detector can be mounted on the spectrometer. The former is mainly used for laboratory performance tests and ground-based measurements. The latter is used for a satellite-borne instrument operated under uncooled condition. The required specifications for this spectrometer are summarized in Table 6-1.

(2) Echelle grating advantage

FTS and grating spectrometers are the most popular instruments in spectrometry. In general the FTS technique has two advantages: Throughput advantage and multiplex advantage. As the solar occultation method is an IFOV limited measurement to achieve the vertical resolution, the former advantage is not effective. A spectrograph by an array detector with a few tens of pixels can cover the $ClONO_2$ baseline like absorption peak. So the latter advantage is not essential in this case. On the other hand, a high spectral resolution FTS is large and heavy with a complicated moving mirror mechanism. Grating array spectrographs have the advantage of rapid measuring intervals and high reliability since they contain no moving parts. It can be concluded that there is no penalty in using a grating spectrometer for solar occultation $ClONO_2$ measurement. Echelle gratings were first developed by Harrison and his group at MIT [*Hutley et al.*, 1990 and *Harrison*, 1949]. They give greater spectral coverage than Fabry-Perot etalons and higher spectral resolution than ordinary gratings. The high dispersion (large blaze angle) of echelle gratings minimizes the size and weight of the instrument. Spectrometers with echelle gratings have an advantage in solar occultation measurements from satellites, which have sufficient radiance but require rapid measuring intervals. Echelle gratings are usually

used in visible and ultra-violet regions for high spectral resolution spectrometry. Since in laboratory IR spectrometers FTS is more commonly used than grating spectrometers, few echelle gratings have been manufactured. An echelle grating was selected from the limited number of stock mother gratings.

The dispersion of a grating spectrometer is described as

$$m\lambda = d\cos i_x \left(\sin i + \sin\beta\right), \tag{6-1}$$

$$\frac{d\lambda}{d\beta} = \frac{d\cos i_x \cos\beta}{m}, \tag{6-2}$$

where m is the diffraction order, λ is the wavelength, d is the groove spacing, i is the incident angle relative to the echelle grating normal, i_x is the incident angle relative to the diffraction surface nominal, and β is the diffraction angle. As the required wavelength region of the measurement is limited, the grating can be mounted in a Littrow configuration. Equation (6-2) then becomes,

$$\frac{d\lambda}{d\beta} = \frac{d\cos i_x \cos\beta}{m} = \frac{t\cos i_x}{m\tan\theta} = \frac{\lambda_b}{2\tan\theta} = \frac{\lambda_b}{2}\frac{s}{t}, \tag{6-3}$$

where θ is the blaze angle, λ_b is the blaze wavelength, t is the step width of the groove, and s is the step height. The ratio t / s of the echelle gratings is normally between 2 and 5, which is larger than the ratio for ordinary gratings. Accordingly echelle-grating spectrometers have larger dispersion. Equation (6-3) also shows that in the Littrow configuration, the resolving power is independent of the diffraction order. However, since the diffraction efficiency is degraded by the polarization effect, it is necessary to carefully select the grating order. Gratings show polarization effects due to the imperfect conductance of their surfaces when the step height of a grating, s, is close to or smaller than the wavelength [*Palmer et al.*, 1993 and *Loewen et al.*, 1995]. It means that a groove step width wider than the wavelength is needed to get high diffraction efficiency. Thus lower groove density gratings give higher diffraction efficiency. The lowest groove density currently available is limited by manufacturing technology to approximately 15 grooves/mm. The strength of the diamond ruling tools limits the depth of the grooves. Other approaches such as manufacturing with a three-dimensional numerical control cutter can be used for lower groove density gratings. The manufacturing requires very high temperature stability and its performance has not yet been tested. The lowest groove density replica among the mother gratings manufactured by the Thermo RGL (former Milton Roy Company) was selected. The groove density is 23.2 grooves per mm and the blaze angle is 65.1 deg. The measured flatness of the grooves was sufficient for thermal IR region spectrometers. With this grating, the diffraction order of spectra at 780.2 cm^{-1} becomes 6 when the optical elements are mounted closely in a Littrow configuration.

The theoretical resolving power of a grating spectrometer at a wavelength λ is given by the Rayleigh criterion to resolve two monochromatic input spectra with equal intensity at wavelength spacing $\Delta\lambda$,

$$\frac{\lambda}{\Delta\lambda} = mN, \tag{6-4}$$

which is proportional to the total number of grooves and the diffraction order. However, because the spectrometer configuration of our design has relatively large pixel size (pyroelectric detector) and a small focal length (space-borne instrument), the resolving power mainly depends on the slit width and detector size rather than theoretical resolving power. Thus the diffraction angle resolution depends on the configuration of the

optics and can be written as

$$\Delta\beta = \frac{l_s}{f_1} = \frac{l_d}{f_2}, \tag{6-5}$$

where l_s is the slit width, f_1 is the focal length of the collimator; l_d is the detector pixel width (pyroelectric detector), and f_2 is the focal length of the collecting mirror. f_1 of this model is 183.8 mm (F =4.6). Thus f_2 is 198.7 mm (F =5.0) and $\Delta\beta$ is 0.001. From equation (6-3) and (6-5), the spectral resolution $\Delta\lambda$ becomes 0.0031 μm . It corresponds to a resolution of 0.189 cm^{-1}.

(3) Optics

The layout of the optics of the spectrometer is shown in Figure 6-2. It is designed to minimize the responsive area of the detector for noise reduction and to achieve good image quality for high spectral resolution. The collimating mirror is an off-axis parabolic mirror to make an ideal collimated input flux to the echelle grating. The two collecting mirrors are off-axis parabolic cylindrical mirrors, which have different focusing speed and a conjugated focal point. The first mirror collects the flux in the dispersion axis and the second one collects the flux in the cross-dispersion axis, which is perpendicular to the dispersion axis. The focusing speed of the dispersion axis is slower to obtain high image quality and a large spectral dispersion. The focal length of the second cylindrical mirror is 45.8 mm (F = 1.1). The focusing speed of the cross-dispersion axis is approximately 4.4 times faster to reduce the area of the detector pixel, which is proportional to the detector noise level. Thus the height to width ratio is 22 at the entrance slit and it reduces to 5 on the focal plane.

The aberration of the slit image is another factor, which limits the spectral resolution. The optical performance is simulated with Code V optical calculation program. Considering the geometry of the slit and the two collecting parabolic mirrors, the best focusing points of the cross-dispersion and the dispersion axis are tilted in different directions from the detector assembly focal plane, which is mounted perpendicular to the optical center axis. Accordingly the slit image spreads slightly on the focal plane. The off-axis angle of the collimating mirror is another major factor resulting in the slit image spread, especially of the slit edge. Figure 6-3 shows the linespread functions at 780.2 cm^{-1} simulated with Code V assuming the optics in Figure 6-2 and a germanium bandpass filter mounted on the detector pixel. These results show that the image quality of the slit center is quite good in both axes and the linespread function shape of the dispersion axis is almost unique. On the other hand, the image of the cross-dispersion axis spreads to the outside of the pixel at the edge. As a result, the overall image quality of the dispersion axis is much better than the cross-dispersion axis. Eighty three percent of the input monochromatic flux is collected on the target pixel.

An echelle grating can overcome polarization effects using a high diffraction order, which is equivalent to a larger groove step width. In general, a combination of fine dispersion by the echelle grating and cross coarse-dispersion by a prism, for example, creates a two-dimensional spectral image, 'echellegram'. In this spectrometer we used a limited spectral region in the 6^{th} order. Since a spectrometer with a cross coarse-disperser is complicated and a cross disperser reduces the optical efficiency, a bandpass filter, which will be described later, was selected to block the orders other than the 6^{th}.

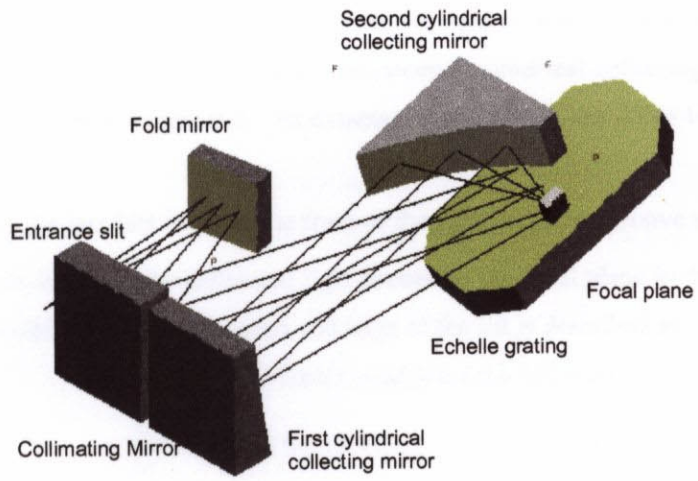

Figure 6-2. Echelle grating spectrometer layout.

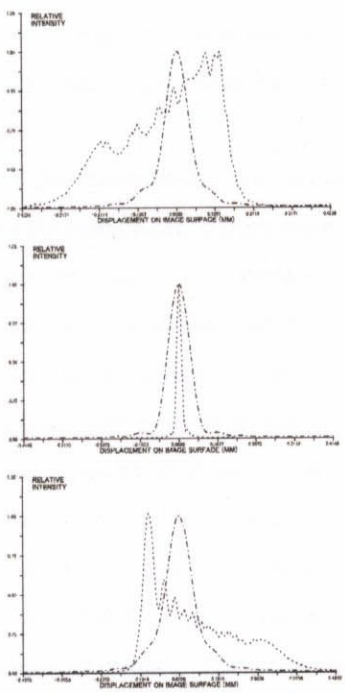

Figure 6-3. Simulated 780.2 cm^{-1} linespread functions on the focal plane. The dash-dotted line and the dotted line are the diffraction intensity profiles of the dispersion axis and the cross-dispersion axis, respectively. From the top, the edge of the slit, the center, and the other edge.

(4) Instrumentation

The designed spectrometer is a modified echelle grating spectrometer, which is optimized for the limited wavelength region spectra. Its specifications are summarized in Table 6-2. A photograph of the flight model is

shown in Figure 6-4. Reflective optics is selected to improve the overall optical efficiency. The grating spectrometer consists of seven elements: (a) entrance slit, (b) fold mirror, (c) collimating mirror, (d) echelle grating, (e) the first cylindrical collecting mirror, (f) the second cylindrical collecting mirror and (g) detector assembly (focal plane) as shown in Figure 6-2. Its dimensions and weight are $290 \times 160 \times 150$ mm and 4.7 kg, respectively.

Entrance slit. As the incident angle to the front of the echelle grating groove step (i_x in Figure 6-5) is not zero (7.5 deg), the slit image of the diffracted light rotates on the focal plane in the Littrow configuration. The relation of the diffracted light from the center and edge of the slit is described as

$$\cos i_x (\sin\beta + \sin i) = \cos(i_x + \Delta i_x)(\sin(\beta + \Delta\beta) + \sin i),$$

$$\frac{\Delta\beta}{\Delta i_x} \cong (tan\, i_x) 2\, tan\, \beta \cong 4\, tan\, i_x \cdot \tag{6-6}$$

Thus to correct the rotation, the relay optics between the foreoptics, which is not described in this chapter, and the echelle grating spectrometer rotates the image on the entrance slit by 30 deg.

Echelle grating. A gold-coated grating surface was to be selected to provide excellent electromagnetic characteristics on the grating surface. Thus the grating has small polarization sensitivity. A ZeroDur grating base, which is tolerant of the temperature cycle in orbit, was also selected. It was mounted on an invar base, which has a small thermal expansion coefficient. The invar base was carefully integrated on the aluminum optical base to minimize bimetal distortion.

Mirrors. The optical elements of the spectrometer are composed of gold-coated mirrors to get high efficiency at 780.2 cm^{-1}. The two parabolic cylindrical mirrors were manufactured by Fuji Photo Optics Co., Ltd. with a three-dimensional numerical control cutter. The surface flatness of the three parabolic mirrors was measured. These results show that the flatness is better than $\lambda/100$ at 780 cm^{-1}. Thus the image quality is not degraded. Each parabolic mirror was mounted as follows. The entrance slit, the collimating mirror and the grating are on the base plate. The grating, the first cylindrical mirror, and the second cylindrical mirror are on the vertical plane. The first and second cylindrical mirrors and the detector are on the inclined plane. Accordingly the image of the slit center has no aberration geometrically.

Detector assembly. As the optical axis on the focal plane optics is parallel to the optical base, the detector assembly is vertically mounted. Both the MCT and pyroelectric detector assemblies are composed of a bandpass filter, detector pixels, and an amplifier circuit. The germanium base bandpass filter was mounted on the detector. It achieves high transmittance at wavelengths of the target diffraction order blocking the other orders. The measured transmittance at 780.2 cm^{-1} is 85% and the bandwidth is 0.85 μm. It blocks wavelengths lower than 12.2 μm and larger than 13.6 μm. The shorter wavelength blocking was carefully designed considering the high input solar radiance in the short wavelength region. The detector signals are processed with a lock-in amplifier the frequency of which is synthesized with the chopper mounted on the entrance slit. Since for the satellite measurements the speed of tangent height change is 3.4 km/sec in orbit and the required height resolution is 1 km, the sampling rate must be faster than 3.4 Hz.

Table 6-2 Design and instrumentation of the echelle grating spectrometer.

Entrance slit Rotated angle	 -30 deg
Optics Collimating mirror Collecting mirror	 Off-axis parabolic F= 4.6 (f = 183 mm) Two cylindrical mirrors off-axis parabolic F= 5.0×1.1 (f = 199×46 mm)
Grating	ZeroDur base , Gold coated
Detector	On-chip bandpass filter

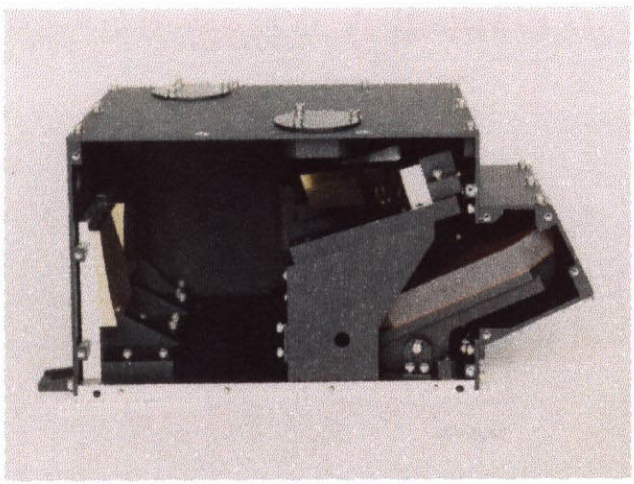

Figure 6-4. View of the flight model.

Environmental design: In general, for satellite-borne instruments, the thermal conditions in orbit and the vibrations endured during launching have to be carefully taken into account. All optical elements except for the grating and its base are made of aluminum (A6061), ensuring that they have the same thermal expansion coefficient. Consequently spectrometric performance will be very stable even when the satellite is in orbit. As there is no special mounting of the optical components and no moving parts in this spectrometer, vibrations are of no concern.

6.3. Performance

The optical components were carefully integrated and the alignment was confirmed with a visible He-Ne laser. The detector assembly was mounted and adjusted on the spectrometer with a cooled IR semiconductor tunable laser. The temperature and current of the semiconductor was precisely controlled. The tuned wavelength was calibrated with a FTS (Bomem DA2) whose highest resolution is 0.022 cm^{-1}.

(1) Slit function

The slit function represents the spectral dispersion and the resolution of the spectrometer. The accurate prelaunch calibration of the slit function is essential for the spectrometer measurement with lower resolution

than the target absorption spectra. To calibrate the slit function in the laboratory, the monochromatic light is generated with the above mentioned tunable diode laser. This laser is strong enough. However its flux is not uniform and the light is coherent. To solve these problems, we use the integrating sphere with diffusive gold inner coating. Figure 6-6 shows the configuration of the slit function measurement. On the other hand we calculated the instrument slit-function by convoluting the point spread function over the slit as follows. (a) The slit is divided into 20 areas. (b) The light from the center of each area is ray-traced onto the focus. (c) The point-spread function of each focused point is simulated with Code V. (d) Then it is convoluted. This simulated slit function has a Gaussian shape. The simulated slit function is in good agreement with the measured one as shown in Figure 6-7.

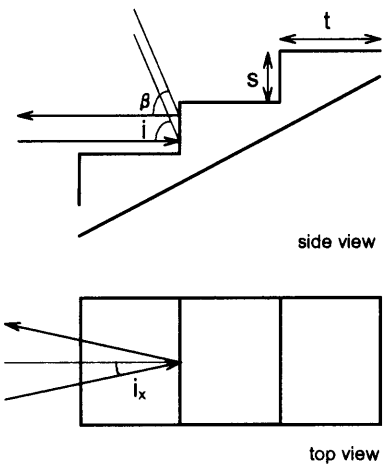

Figure 6-5. Incident and diffraction angles of the echelle grating.

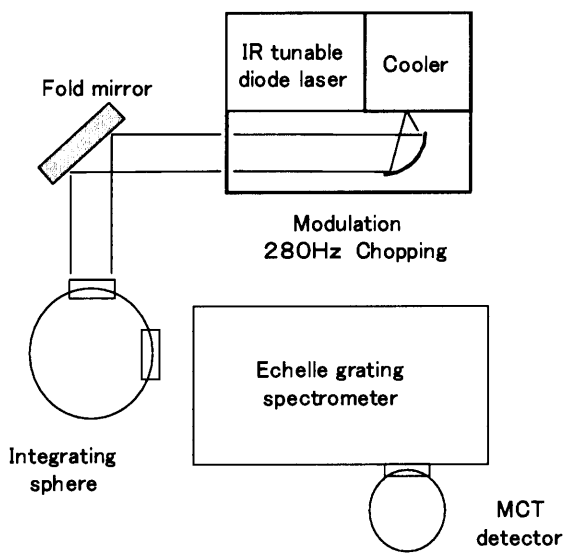

Figure 6-6. Configuration of the slit function measurement.

(2) Signal-to-noise ratio

The SNR of the MCT output signal of solar spectra was also measured on the ground. It was

approximately 1000 when the outputs of 2 pixels were added. The SNR of this spectrometer mainly depends on the input flux photon amount and the detector noise. The input scene flux is described as

$$S = L\,\Theta\,T\,\Delta\nu, \tag{6-7}$$

where S is the input scene flux, L is the target spectral radiance, Θ is the throughput, T is the overall efficiency of the optics including the eclipse of the telescope, grating diffraction efficiency and bandpass filter transmittance, and $\Delta\nu$ is the spectral bandwidth. As previously discussed, the pixel responsive area is designed to be small to reduce the detector noise level. When solar spectral radiance L (780.2 cm^{-1}) in orbit is 28 $W/m^2/sr/cm^{-1}$, Θ is $2.3\times10^{-8} m^2 sr$, T is 0.4 and $\Delta\nu$ is 0.189 cm^{-1}, the calculated input scene flux becomes $4.9\times10^{-8} W$. The signal-to-noise ratio (SNR) is estimated as follows,

$$SNR = \frac{SD^*}{A^{1/2}\,\Delta f^{1/2}}, \tag{6-8}$$

where D^* is specific detectivity including circuit noise, A is the pixel responsive area, and Δf is the sampling frequency bandwidth. The D^* of the pyroelectric detector and the MCT detector are $8.0\times10^{7} cm\,Hz^{1/2}/W$ and $1.3\times10^{9} cm\,Hz^{1/2}/W$, respectively. The pyroelectric detector has the same pixel responsive area as the slit image without aberration, which is $1.8\times10^{-3} cm^2$ and the MCT has about the half size pixel as listed in Table 6-1. When the sampling frequency is 3.4 Hz (1.7 Hz bandwidth), the estimated SNR is 64 for the pyroelectric detector. It becomes 980 for the MCT detector when the outputs of 2 pixels are added.

(3) Ground-based measurements

Figure 6-8 shows the measured solar spectra with a one-dimensional MCT array detector on 16 October 1996 in Yokohama, Japan. H_2O and CO_2 absorption spectra near the 780.2 cm^{-1} spectral region are detected clearly on the ground. For comparison the 0.2 cm^{-1} resolution spectra were also acquired simultaneously with a FTS (Bomem DA2). The data measured with this echelle grating spectrometer are in good agreement with the FTS data and FASCODE calculated results. The calculated data are convoluted with the simulated slit function. These results show that the echelle grating spectrometer has a 0.189 cm^{-1} spectral resolution as designed with sufficient SNR.

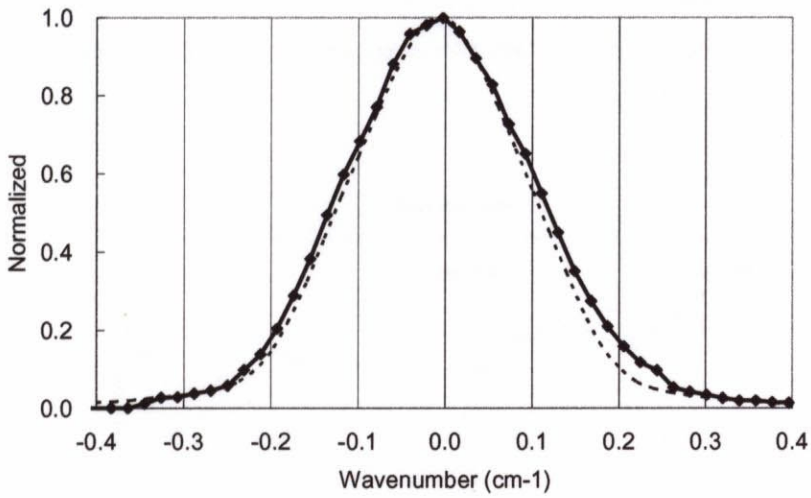

Figure 6-7. Comparison of measured (solid curve) and simulated (dotted curve) slit function.

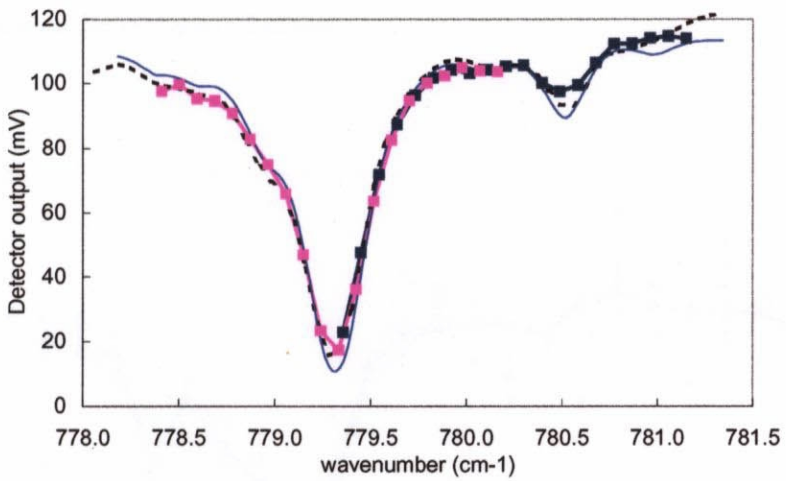

Figure 6-8. Measured H_2O and CO_2 absorption spectra in Yokohama, Japan, at noon, 16 October 1996 (bold curve) compared with data with Bomem DA2 FTS (dotted curve) and FASCODE numerical simulation (solid curve).

(4) Performance with thermal detector (pyroelectric detector)

Cooled array MCT detector has enough detectivity to characterize the instrument function. However, the pyroelectric (thermal) detector is used for onboard configuration, which has less detectivity than MCT and twice as large pixel size. Figure 6-9 shows the expected measured data on board using a pyroelectric detector. It is the convoluted value of the absorption spectra of O_3, H_2O and $ClONO_2$ and instrument function. As the pyroelectric detector has twice as large pixel width as MCT, the spectral resolution is degraded. Figure 6-10 shows the variation of the ground data and due to the lower detectivity of the thermal detector, measured SNR is around 15 on the ground, which is lower than the expected SNR of around 50 on board due to the aperture

limitation of the test configuration on the ground. However, as the noise is white, by averaging the acquired spectra, the precision is increased and the spectra agree with the FTS (DA2) of 0.2 cm^{-1} resolution mode as shown in Figure 6-11.

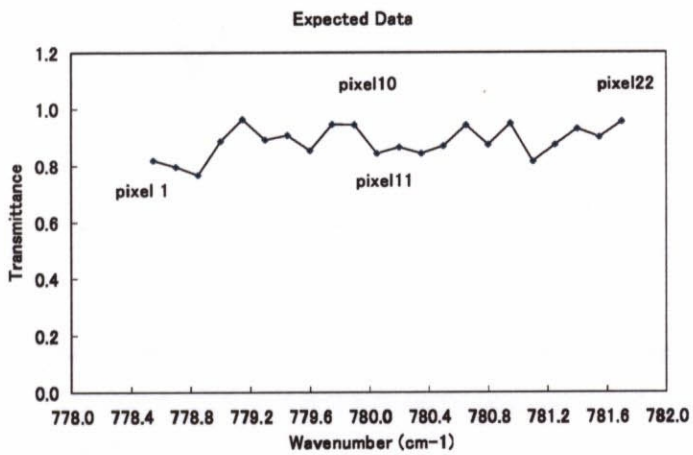

Figure 6-9. Expected measured data on board with pyroelectric detector, which is convoluted with the instrument function.

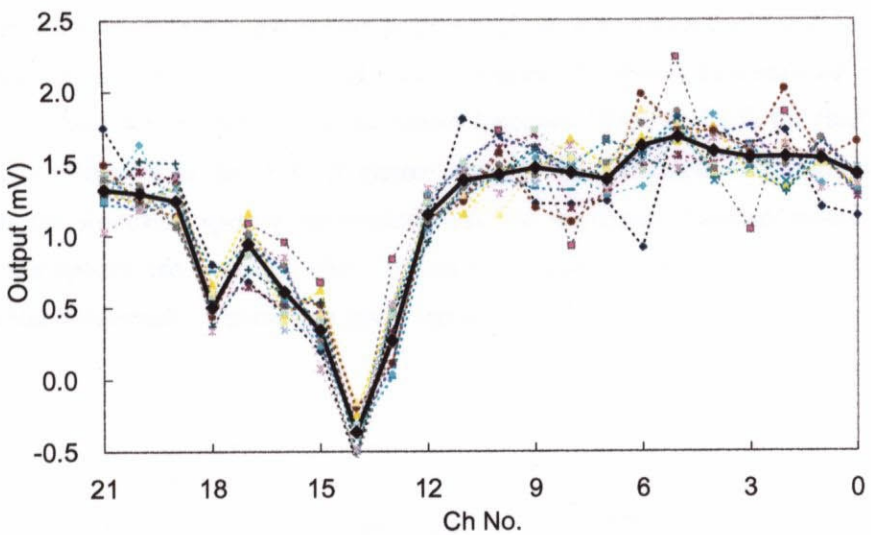

Figure 6-10. Variation of measured H_2O and CO_2 absorption spectra (15 samples) using pyroelectric detector in Yokohama, 30 October 1997 after collection the response variation between pixels (dotted lines) compared with averaged value (bold solid line).

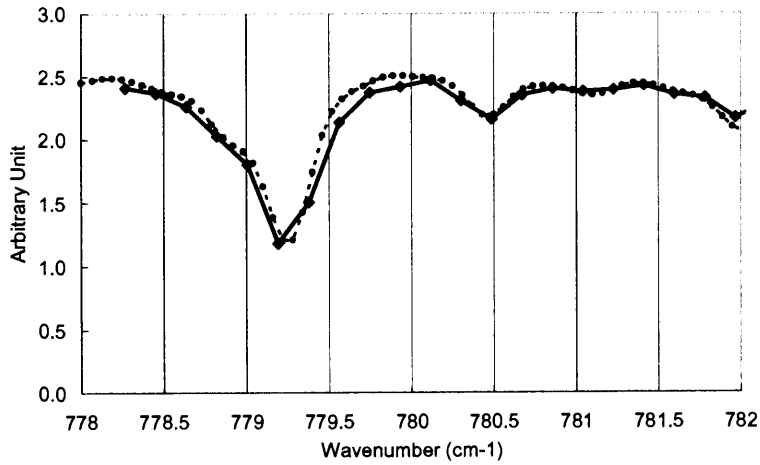

Figure 6-11. Averaged measured H_2O and CO_2 absorption spectra using pyroelectric detector at 10:15 on 3 December 1996 at Yokohama (solid line) compared with data with Bomem DA2 FTS (dotted line).

(5) Performance validation with gas cell

The other method to validate the instrument function characterization is to use gas cell. The kind of sample gases, which have absorption spectra in this region, is limited. C_2H_6 has absorption in this spectral region, however, the intensity and width are not large enough to characterize the instrument function. In this case the 1m long cell is filled with the CO_2 of 1 atm. Figure 6-12 shows the simulated transmittance of the CO_2 absorption without convolution of the instrument function. Figure 6-13 is the final test data after the echelle grating is integrated to the ILAS-II system acquired by Matsushita Communication Industrial and compared with the simulated spectra convoluted with the instrument function model. As in the final configuration, the spectra are acquired with a pyroelectric detector, they are noisy. However, weak CO_2 absorption is clearly detected. On orbit in polar region $ClONO_2$ absorption is expected to be stronger than CO_2.

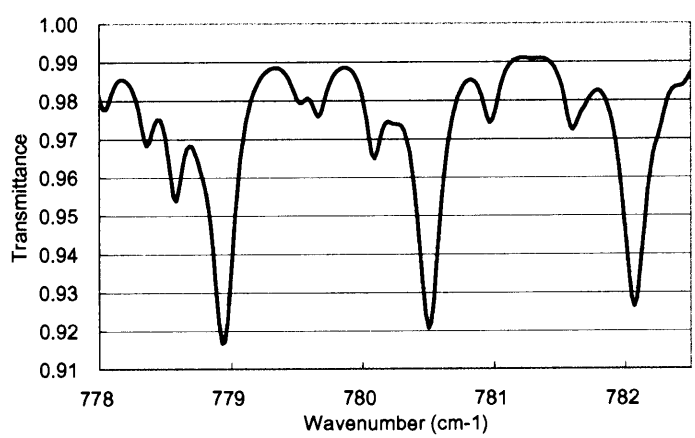

Figure 6-12. Simulated absorption spectra of CO_2 by FASCODE3P.

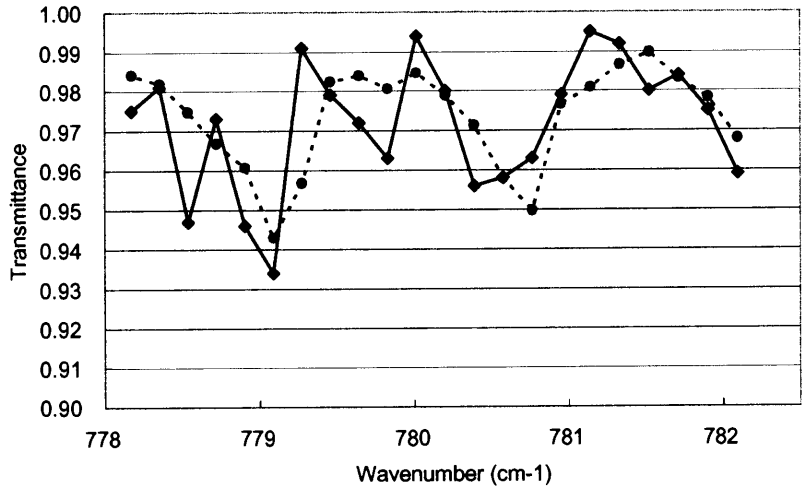

Figure 6-13. Measured absorption spectra (solid line) of 1m gas cell with CO_2 with flight model final configuration compared with simulated data convoluted with the model instrument function (dotted line).

6.4. Discussion

As the radiance of the artificial light source is mush smaller than the one of the sun and the optical path of the gas cell is limited in the laboratory, the test with gas cell requires very high SNR. For the composition measurements of the less abundant or narrow spectral width, higher signal to noise ratio is required. In this case, the thermal detector must be replaced by the quantum one such as MCT.

6.5. Conclusion of this Chapter

A small, lightweight, space-borne solar occultation instrument, making use of an echelle grating spectrometer with the following characteristics, has been designed and tested:

(a) High spectral dispersion with an echelle grating

(b) Minimized pixel responsive area with two cylindrical collecting mirrors

(c) High quality of the image with three parabolic mirrors

(d) High overall optical efficiency with gold-coated reflective optics, high diffraction efficiency grating and high transmittance bandpass filter

(e) High reliability since it is without a scanning mechanism

(f) Rapid measuring intervals

The performance of this flight model has been confirmed. It meets the environmental condition requirements of the ADEOS-II satellite. It is concluded that an echelle grating spectrometer is an adequate satellite-borne instrument for measuring a specific molecule.